Applied Catalysis A: General 443–444 (2012) 33–39

Contents lists available at SciVerse ScienceDirect

Applied Catalysis A: General

journal homepage: www.elsevier.com/locate/apcata

Acidic characterization and activity of $(NH_4)_xCs_{2.5-x}H_{0.5}PW_{12}O_{40}$ catalysts in the esterification reaction of oleic acid with ethanol

Joicy S. Santos, José A. Dias*, Sílvia C.L. Dias, Julio L. de Macedo, Fillipe A.C. Garcia, Liana S. Almeida, Eduardo N.C.B. de Carvalho

Universidade de Brasília, Campus Universitário Darcy Ribeiro, Asa Norte, Instituto de Química, Laboratório de Catálise, Caixa Postal 4478, Brasília, DF, 70904-970, Brazil

ARTICLE INFO

Article history:
Received 23 March 2012
Received in revised form 11 July 2012
Accepted 14 July 2012
Available online 21 July 2012

Keywords:
Acidity
Heteropoly salts of cesium and ammonium
Thermal stability
Gas phase pyridine adsorption
12-Tungstophosphoric acid
Nanostructured catalyst
Esterification
Oleic acid
Ethanol

ABSTRACT

Ammonium and cesium derivatives from $H_3PW_{12}O_{40}$ (H_3PW), namely $(NH_4)_xCs_{2.5-x}H_{0.5}PW_{12}O_{40}$ ($x = 0.5$, 1, 1.5, 2), were synthesized and structurally characterized by FT-Raman spectroscopy, and their thermal stability was evaluated by FTIR and TGA/DTA. The acidity was characterized by the adsorption/desorption of gaseous pyridine, by FTIR and TGA/DTA as well as by the reaction of oleic acid and ethanol. The stability of the mixed salts regarding the Keggin structure was much higher than the parent acid, with the onset decomposition around 520 °C. Nonetheless, calcination up to 300 °C is recommended for the integrity of the mixed salt. The FTIR of adsorbed pyridine displayed only Brønsted acidic sites, which was confirmed by TGA measurements of the formation of $Py{-}H^{+}\cdots Py$ adducts. The best esterification result was for $(NH_4)_2Cs_{0.5}H_{0.5}PW_{12}O_{40}$ with TOF = 1.314 mol_{EO} mol^{-1} proton s^{-1} with a 1:6 (oleic acid:ethanol) molar ratio, at 80 °C and 10 wt% catalyst in relation to the acid.

1. Introduction

Polyoxometalates (POMs) are a class of clusters with a unique range of physical and chemical properties [1]. These materials can be used in a variety of technological fields, but their use as catalysts continues to be their most common application. POMs with Keggin structures are the most disseminated type of catalyst and are used for a wide range of organic reactions (e.g., multi-component, oxidation, reduction, electrochemical, photochemical) [2]. Their use has been evaluated not only for bench-scale laboratory research but also for large-scale industrial processes [1–3]. Among the various POMs, 12-tungstophosphoric acid ($H_3PW_{12}O_{40}$, H_3PW), along with its salt derivatives, is the most studied material for acidic reactions because it is the strongest heteropolyacid in the series [4].

Biodiesel is the name given to long-chain alkyl esters derived from biomass feedstock [5,6]. It is a plausible substitute for petroleum diesel because it is obtained from renewable sources. It is attractive as an alternative fuel not only because of its environmental benefits (e.g., biodegradability, low emission profiles), but also due to the possibility of producing biodiesel using second-generation resources [7]. In light of green processes, the use of heterogeneous catalysts is preferable to that of homogeneous catalysts [8]. Among several catalysts tested for biodiesel production, the POMs stand out [9], such as in the studies of Giri et al. [10] about the esterification of palmitic acid with methanol over the ammonium salt of H_3PW. Kulkarni et al. [11] achieved biodiesel production through the simultaneous esterification and transesterification of a mixture of rapeseed oil and oleic acid (90:10 wt% proportion) with ethanol, using H_3PW supported on diverse oxides. Morin et al. [12] reported the transesterification of rapeseed oil with methanol and ethanol utilizing heteropolyacids, such as H_3PW, 12-tungstosilicic acid (H_4SiW) and 12-molybdophosphoric acid (H_3PMo), as catalysts. Narasimharao et al. [13] tested a series of $Cs_xH_{3-x}PW_{12}O_{40}$ salts ($x = 0.9–3$) and found that they were active for esterification of palmitic acid and transesterification of tributyrin. Chai et al. [14] produced biodiesel using $Cs_{2.5}H_{0.5}PW_{12}O_{40}$ as catalyst. They have used the oil of *Eruca sativa* Gars (ESG, a kind of crucifer plant) for the transesterification reaction with methanol. A study by Sunita et al. [15] reported the production of biodiesel by the transesterification of sunflower oil with methanol, using zirconia-supported isopoly and heteropoly tungstates. Cardoso et al. [16] used H_3PW as a homogeneous catalyst to promote the esterification of different saturated and unsaturated fatty acids (myristic, palmitic, stearic, oleic and linoleic) under mild reaction

* Corresponding author. Tel.: +55 61 3107 3846; fax: +55 61 3368 6901.
E-mail address: jdias@unb.br (J.A. Dias).

0926-860X/$ – see front matter © 2012 Elsevier B.V. All rights reserved.
http://dx.doi.org/10.1016/j.apcata.2012.07.013

conditions. Caetano et al. [17] studied the esterification of palmitic acid with methanol using H_3PW, H_3PMo and H_4SiW immobilized by sol–gel technique on silica, at 60 °C. Xu et al. [18] prepared a mesoporous composite catalyst of H_3PW/Ta_2O_5, and applied it as a solid acid catalyst for the esterification reaction of lauric acid with ethanol. These examples demonstrate the strong interest in POMs for esterification and transesterification processes.

Novel mixed salts of cesium and ammonium derivatives of H_3PW ($(NH_4)_xCs_{2.5-x}H_{0.5}PW_{12}O_{40}$, abbreviated thereinafter as $(NH_4)_xCs_{2.5-x}H_{0.5}PW$) have recently been synthesized and characterized [19]. During the synthesis, the primary nanoparticles aggregated, forming structures with mesopores and micropores. The pores were created by partial unidirectional growth of the nanocrystals during the formation of larger, round microcrystallites, leading to materials with higher surface area and lower solubility than the parent acid. These properties are important for surface-type catalysis and liquid phase-separation purposes.

The goal of this work is to study the thermal stability and acidity of these mixed salts of ammonium and cesium derivatives of H_3PW and to apply them to the esterification reaction with ethanol. The mixed salts were characterized by FT-Raman to confirm their structures and their stability was evaluated by calcination followed by FTIR and thermal analysis. The nature of the acid sites was accessed by adsorption of gaseous pyridine detected by FTIR. The amount and strength of the sites were calculated by desorption of pyridine, measured by thermal analysis. The catalytic activities of the mixed salts were tested on the model esterification reaction of oleic acid with ethanol.

2. Experimental

2.1. Preparation of the ammonium and cesium mixed salts of H_3PW

The mixed salts were synthesized by the precipitation method, which consisted of the addition of $(NH_4)_2CO_3$ (Vetec) to H_3PW (Sigma) followed by Cs_2CO_3 (Aldrich), leading to the salts $(NH_4)_xCs_{2.5-x}H_{0.5}PW$ (x = 2, 1.5, 1, 0.5): $(NH_4)_2Cs_{0.5}H_{0.5}PW$, $(NH_4)_{1.5}Cs_1H_{0.5}PW$, $(NH_4)_1Cs_{1.5}H_{0.5}PW$ and $(NH_4)_{0.5}Cs_2H_{0.5}PW$. The samples were prepared by adding pre-determined amounts of a 0.20-mol L^{-1} aqueous solution of the carbonates (freshly prepared) to a 0.08-mol L^{-1} fresh solution of H_3PW (at a rate of 1 mL min^{-1}). The stoichiometry was in agreement with Eqs. (1)–(4):

$$(NH_4)_2CO_3 + 0.25Cs_2CO_3 + H_3PW_{12}O_{40} \rightarrow (NH_4)_2Cs_{0.5}H_{0.5}PW_{12}O_{40} + 1.25CO_2 + 1.25H_2O \quad (1)$$

$$0.75(NH_4)_2CO_3 + 0.5Cs_2CO_3 + H_3PW_{12}O_{40} \rightarrow (NH_4)_{1.5}Cs_{1.0}H_{0.5}PW_{12}O_{40} + 1.25CO_2 + 1.25H_2O \quad (2)$$

$$0.5(NH_4)_2CO_3 + 0.75Cs_2CO_3 + H_3PW_{12}O_{40} \rightarrow (NH_4)_{1.0}Cs_{1.5}H_{0.5}PW_{12}O_{40} + 1.25CO_2 + 1.25H_2O \quad (3)$$

$$0.25(NH_4)_2CO_3 + Cs_2CO_3 + H_3PW_{12}O_{40} \rightarrow (NH_4)_{0.5}Cs_{2.0}H_{0.5}PW_{12}O_{40} + 1.25CO_2 + 1.25H_2O \quad (4)$$

The solution was aged overnight at 25 °C, evaporated to dryness at 40–50 °C and ground into fine particles in a mortar for further calcination. Other details of this preparation and complete characterization can be found elsewhere [19].

2.2. Characterization of the catalysts

Infrared spectra of the mixed salts and the pyridine-adsorbed POMs were obtained with a Thermo Scientific Nicolet spectrometer model 6700 FTIR with 128 scans and a spectral resolution of 4 cm^{-1}. Each sample was pressed in dried 1-wt% KBr (Merck) pellets.

FT-Raman spectra were recorded on a Bruker FRA 106/S module attached to a Bruker Equinox 55 spectrometer (128 scans and 4 cm^{-1} resolution). The laser excitation (Nd:YAG = neodymium:yttrium aluminum garnet) and laser power were 1064 nm and 250 mW, respectively, and the signal was detected by a liquid N_2-cooled Ge detector. Samples without any thermal treatment were packed into sample cups for analysis. For liquid samples (reaction products), a 1-cm quartz cuvette with a mirror surface toward the scattering direction was used.

Thermal analysis consisted of thermogravimetric (TGA), derivative thermogravimetric (DTG) and differential thermal analysis (DTA). They were obtained in a simultaneous TG-DSC (TA Instruments, model SDT 2960), with a heating rate of 10 °C min^{-1}, from room temperature (~25 °C) up to 800 °C under a synthetic air (80.0 ± 0.5% N_2 and 20.0 ± 0.5% O_2) flow of 110 mL min^{-1}.

2.3. Thermal activation of the catalysts

After preparation, the catalysts underwent different heating treatments for the thermal stability studies: 200, 300, 450 and 650 °C for 4 h in a muffle furnace (EDG model EDG3PS) under static air conditions at a heating rate of 10 °C min^{-1}. Before the catalytic tests, the materials were activated at 200 °C for 4 h in the same furnace.

2.4. Gas phase adsorption of pyridine

Fresh pyridine (Vetec) was purified by distillation over CaH_2 (Merck) using a 12 in. Vigreux column and stored under 3A molecular sieves. The gas-phase pyridine (Py) adsorption was conducted simultaneously for all POMs. Platinum crucibles loaded with the samples (~20 mg) were placed in a shallow porcelain plate and inserted into a glass tube inside a tubular furnace (Thermolyne, model F21135). The catalysts were dehydrated in dried N_2 (100 mL min^{-1}) at 200 °C for 1 h. The system was then cooled to 100 °C and gaseous pyridine diluted with N_2 was allowed to pass through the samples for 1 h. Finally, the temperature was held at 150 °C under N_2 for 2 h to remove any physically adsorbed pyridine. The samples with adsorbed pyridine were analyzed by TG/DTG and FTIR.

Acidity was obtained by TG/DTG data, as explained below. The total number of acid sites (n_{Py}) was determined by quantitative analysis of TG/DTG curves of the catalysts before (Sample) and after pyridine adsorption (Sample-Py), according to Eq. (5)

$$n_{Py}\ (\text{mmol}) = \frac{\overbrace{(m_{700}/(m_{total} - m_{200}))}^{\text{Sample-Py}} - \overbrace{(m_{700}/(m_{total} - m_{200}))}^{\text{Sample}}}{MM_{Py}} \times 1000 \quad (5)$$

First, it is determined the difference between the total mass (m_{total}) of a sample (containing pyridine) and the mass loss (m_{200}) between room temperature (25 °C) and 200 °C (i.e., the range of temperature where there are losses of water and any remainder physically adsorbed pyridine). This difference is related to the anhydrous sample with pyridine chemically adsorbed. Then, the mass loss (m_{700}) between 200 and 700 °C is normalized to a gram, dividing this mass (m_{700}) by that difference ($m_{total} - m_{200}$). Accordingly, the same method is applied to the sample without pyridine (i.e.,

pure sample before pyridine adsorption experiment). Thus, the subtraction of the normalized masses ($Sample_{Py}$ – Sample) gives the adsorbed pyridine on the solid sample. Finally, the mass is converted to mmol of pyridine (n_{Py}) dividing by the molar mass of pyridine (MM_{Py}) and multiplying by 1000.

2.5. Catalytic tests

Oleic acid (Vetec, 99%) was used without further purification. Ethanol (Vetec, 99.8%) was further purified with 3A molecular sieves (Aldrich) for at least 24 h before the experiments. The esterification reaction was performed in a 50 mL glass round-bottom flask connected to a reflux condenser (kept at 15 °C by a refrigerated circulating bath – Lauda, K-2/R). The system was kept stirring at 80 °C using an oil bath over a digital stirring hot plate (Corning, PC-420D). The flask contained 1 g of oleic acid, 0.1 g of catalyst (10 wt%) and variable amounts of ethanol (4.89, 2.45 and 0.98 g) relative to 1:30, 1:15 and 1:6 molar ratios (oleic acid:ethanol), respectively. The course of the reaction was analyzed at different time periods (1, 2, 4 and 6 h). At the end of each reaction period, the system was cooled to room temperature and the solid catalyst was filtered out of the reaction products. The products were then extracted three times with a 5-wt% solution of NaCl, dried over magnesium sulfate and kept overnight in a desiccator to remove residual alcohol. The conversion of oleic acid to ethyl oleate was analyzed using a Raman/PLS calibration model, similar to that described by Ghesti et al. [20]. The calculated conversions are within ±5% error (twice the standard deviation of a triplicate determination). In all cases, 100% selectivity to ethyl oleate was observed for this reaction, as shown by either GC/FID, GC/MS or ^{1}H NMR analyses.

The reactions were initially tested for mass diffusion limitations using different stirring rates. A stirring of 1000 rpm was enough to keep the same yield for the model reaction studied. Also, different amounts of catalyst were checked (10 and 15 wt% catalyst) and the results did not show any mass transfer limitations (proportional yields as the catalyst amount increased).

The calculation of the turnover frequency (TOF) was based on the following procedure: first, a curve of the yield of the product (mmol) versus time (s) was plotted for each catalyst; then, the initial activity of each catalyst was determined from that plot of ester produced versus time, which was fitted to a third-order polynomial function. The obtained function was differentiated, evaluated at $t = 0$ and divided by the number of theoretical protons of each catalyst (taking into consideration the molecular formula of each mixed oxide and the mass of the catalyst in each reaction, i.e., 0.1 g) to determine the respective TOF ($mmol_{ethyl\ oleate\ (EO)}\ mmol^{-1}\ proton\ s^{-1}$).

3. Results and discussion

3.1. Basic structural characterization

The integrity of the catalysts was evaluated by FTIR and FT-Raman spectroscopy. FTIR results show the maintenance of the Keggin structure through the fingerprint absorptions [19]: ν_{as}(P—O) at 1080 cm^{-1}, ν_{as}(W=O) at 983 cm^{-1}, ν_{as}(W—O_c—W) at 893 cm^{-1} and ν_{as}(W—O_e—W) at 798 cm^{-1}. The δ(O—P—O) at 550 cm^{-1}, N—H stretching at 1420 cm^{-1} and O—H bending assigned to the presence of water in the outer solvation sphere around 1615 cm^{-1} lend further support to this observation.

The FT-Raman spectra of H_3PW show a set of bands at 1011, 996, 900 and 550 cm^{-1} (Fig. 1). The first two bands are linked to the symmetric and asymmetric stretching of W=O_t, while the other bands are related to the bending modes of W—O_c—W and O—P—O, respectively. These bands confirm the presence of the Keggin structure in the synthesized materials [21,22]. A Raman vibration band at 217 cm^{-1}, which is correlated with the strength of W—O—W bridges, was also observed [23]. This band allows the evaluation of the bond strength of Keggin's anion corner oxygen atoms, which are related to the electrostatic interaction of the neighbor anions with different cations [22].

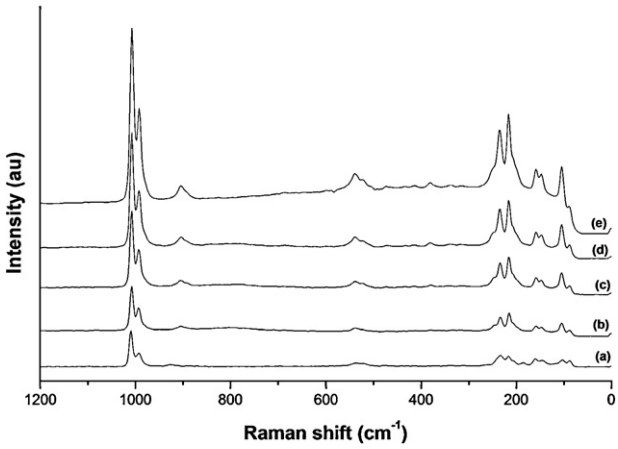

Fig. 1. FT-Raman spectra of (a) H_3PW, (b) $(NH_4)_{0.5}Cs_2H_{0.5}PW$, (c) $(NH_4)_1Cs_{1.5}H_{0.5}PW$, (d) $(NH_4)_{1.5}Cs_1H_{0.5}PW$ and (e) $(NH_4)_2Cs_{0.5}H_{0.5}PW$, all before calcination.

3.2. Thermal stability

DTG (Fig. 2) and DTA (Fig. 3) curves were simultaneously obtained for H_3PW and its mixed salts. An initial mass loss in the range of 25–110 °C is observed in all samples (Fig. 2), which is related to the release of physically adsorbed water and part of the hydrated water (e.g., formation of $H_3PW{\cdot}6H_2O$ and the respective hydrated salts). The temperature range and the maximum mass loss temperature may vary according to the amount of water contained in each material because heteropolyacids are known to absorb different amounts of water depending on preparation method and storage conditions [24]. The water desorption process is endothermic, as exhibited by the DTA curve (Fig. 3). A second mass loss occurs from 110 to 230 °C (Fig. 2), with about the following maxima: 175 °C (H_3PW); 150 °C ($(NH_4)_{0.5}Cs_2H_{0.5}PW$ and $(NH_4)_1Cs_{1.5}H_{0.5}PW$); 140 °C ($(NH_4)_{1.5}Cs_1H_{0.5}PW$); and 160 °C ($(NH_4)_2Cs_{0.5}H_{0.5}PW$). These maxima are associated with the formation of the anhydrous catalysts. This water probably desorbs from the coordination sphere of the cations and the micropores of each

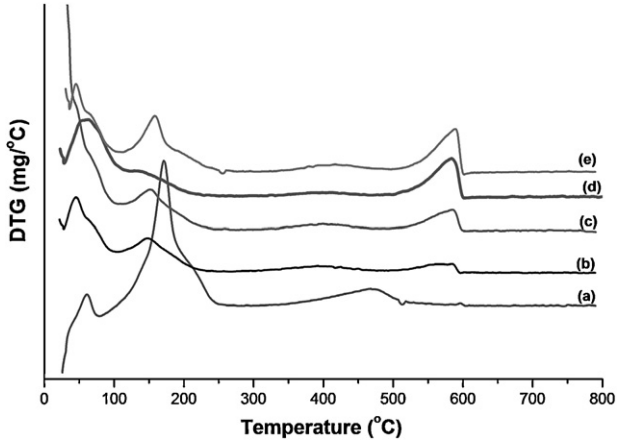

Fig. 2. DTG curves of (a) H_3PW, (b) $(NH_4)_{0.5}Cs_2H_{0.5}PW$, (c) $(NH_4)_1Cs_{1.5}H_{0.5}PW$, (d) $(NH_4)_{1.5}Cs_1H_{0.5}PW$ and (e) $(NH_4)_2Cs_{0.5}H_{0.5}PW$, all after calcination at 200 °C/4 h.

Table 1
Properties of H_3PW and the mixed salts of $(NH_4)_xCs_{2.5-x}H_{0.5}PW$ after calcination at 200 °C for 4 h under air.

Catalyst	S_{BET} [a] ($m^2\,g^{-1}$)	S_{micro} [b] ($m^2\,g^{-1}$)	S_{meso} [c] ($m^2\,g^{-1}$)	P_s [d] (nm)	V_p [e] ($cm^3\,g^{-1}$)	n_{H_2O} [f] (mol)	Acidity[g] (mmol g^{-1})	TOF[h]
H_3PW	4.8	n.a.	n.a.	7.1	n.a.	22.1	1.03	0.021
$(NH_4)_{0.5}Cs_2H_{0.5}PW$	33.5	27.0	6.5	2.2	0.001	4.7	0.36	0.039
$(NH_4)_1Cs_{1.5}H_{0.5}PW$	33.7	24.9	8.8	3.0	0.004	7.4	0.40	0.976
$(NH_4)_{1.5}Cs_1H_{0.5}PW$	44.0	26.3	17.7	3.2	0.014	5.5	0.39	1.293
$(NH_4)_2Cs_{0.5}H_{0.5}PW$	46.1	21.7	24.4	3.4	0.023	5.4	0.41	1.314

[a] Average error is less than ±4% for 3σ (R^2 = 0.999).
[b] Micropore area calculated by *t*-plot.
[c] Estimated as: $S_{meso} = S_{BET} - S_{micro}$.
[d] BJH desorption average pore width ($4V/A$).
[e] BJH desorption cumulative volume of pores.
[f] Actual number of moles of H_2O before calcination of POMs, obtained by TGA.
[g] Total acidity calculated by pyridine desorption (TGA/DTG). For H_3PW, this is a theoretical value.
[h] Turnover frequency = ($mol_{EO}\,mol^{-1}$ proton s^{-1}).

salt and it is also an endothermic step (Fig. 3). The total amount of water released is much lower for the mixed salts than H_3PW, as expected by their respective hydration degrees (Table 1). A third mass loss takes place between 400 and 510 °C with a maximum around 460 °C for pure H_3PW. This process has been associated with the initial decomposition of the Keggin structure by the release of structural water, i.e., water originating from the oxygen of the lattice and acidic protons [24]. This mass loss ranges from 350 to 510 °C for the mixed salts and is related to the release of ammonia from ammonium decomposition. A fourth mass loss is observed for the mixed salts in the range of 520–610 °C. The total decomposition of the Keggin structure is represented in the DTA curves by sharp exothermic peaks at maximum temperatures around 600 °C, which forms the more stable oxides of Cs_2O, WO_3 and P_2O_5 [24–26].

Pure H_3PW starts the Keggin anion decomposition at about 460 °C. The prepared mixed salts showed the analogue decomposition around 580 °C. This result was in agreement with others, which reported that salts of potassium, cesium or ammonium derivatives of H_3PW are thermally more stable materials than the parent acid [27,28]. To check for structural changes on the mixed salts along the range of temperatures covered by TGA/DTA experiments, FTIR spectra of these materials were acquired after calcinations at 200, 300, 450 and 650 °C. A representative spectrum at each calcination temperature is shown in Fig. 4 for $(NH_4)_2Cs_{0.5}H_{0.5}PW$ salt. It was observed that the four Keggin bands (1080, 983, 893 and 798 cm^{-1}) decreased their intensities as the calcination temperature raised. At 650 °C, these bands became very broad, which indicated a partial decomposition of the Keggin anion. The other characteristic that changed was the intensity of the N-H absorption at 1420 cm^{-1}. At temperatures above 300 °C this band started to decrease, indicating a decomposition of ammonium ion into ammonia keeping the proton in the structure. The other mixed salts also showed similar behavior (Figs. S1–S3). These data confirmed the TGA/DTA results and indicated that the best choice to keep not only the integrity of the Keggin anion, but also the correct stoichiometric composition of the salts should be calcination at temperatures up to 300 °C. These structural behaviors upon thermal treatments have also been observed for pure cesium salt derivatives of H_3PW [29].

3.3. Gaseous pyridine adsorption

Samples of the mixed salts were submitted to adsorption of gaseous pyridine and characterized by FTIR and TG to analyze the nature of the acidic sites and to quantify the total amount of pyridine adsorbed on each POM. The FTIR spectra of the mixed salts after pyridine adsorption show that the structure was maintained for all of the salts (Fig. S4), as attested by the Keggin fingerprint and the ammonium-ion band for each salt. The typical region of adsorbed pyridine (Fig. 5) is observed with the following bands: 1638, 1610, 1540, 1487, 1420 and 1384 cm^{-1}. The band at 1610 cm^{-1} is attributed to the second mode of pyridine adsorption on Brønsted sites, which is reinforced by the presence of absorptions at 1638, 1540 and 1487 cm^{-1} also related to this specific site [30]. The absorption at 1420 cm^{-1} is due to N—H bending in the materials and its intensity is roughly proportional to the amount of ammonium in the mixed salts. The absorption at 1384 cm^{-1} is due to a pyridine molecule bonded to another pyridine molecule by

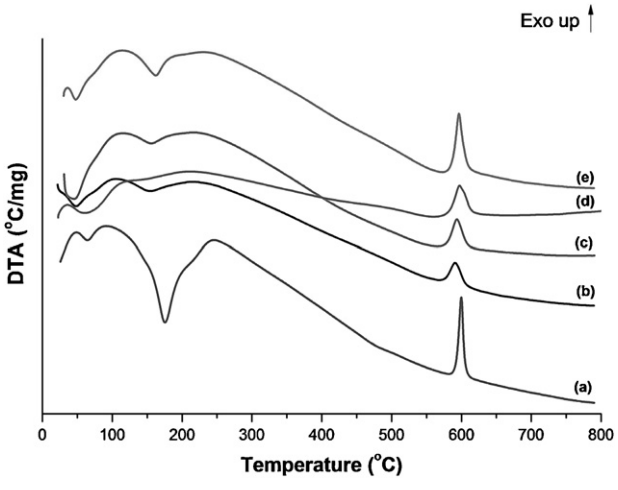

Fig. 3. DTA curves of (a) H_3PW, (b) $(NH_4)_{0.5}Cs_2H_{0.5}PW$, (c) $(NH_4)_1Cs_{1.5}H_{0.5}PW$, (d) $(NH_4)_{1.5}Cs_1H_{0.5}PW$ and (e) $(NH_4)_2Cs_{0.5}H_{0.5}PW$, all after calcination at 200 °C/4 h.

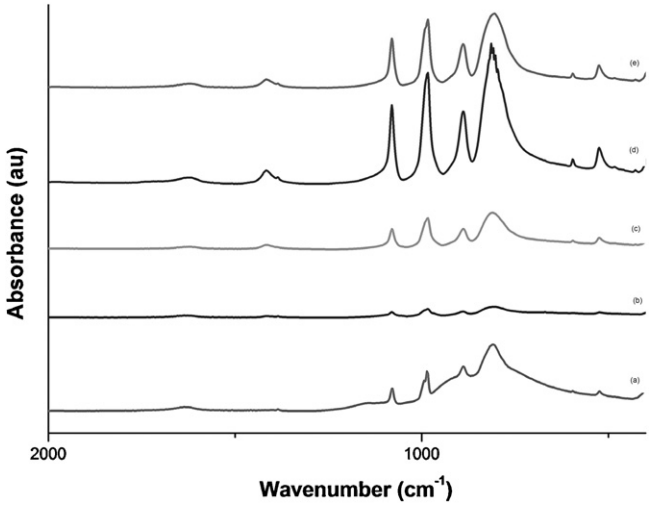

Fig. 4. FTIR spectra of $(NH_4)_2Cs_{0.5}H_{0.5}PW$ after calcination at (a) 650 °C, (b) 450 °C and (c) 300 °C and (e) without calcination.

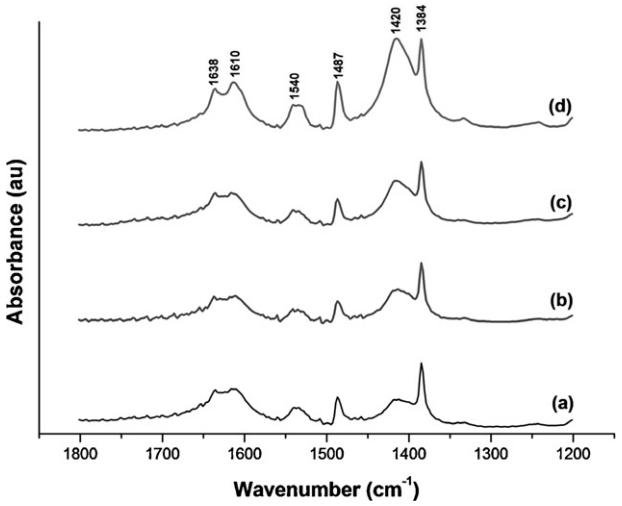

Fig. 5. FTIR spectra of the following mixed salts after pyridine adsorption treatment: (a) $(NH_4)_{0.5}Cs_2H_{0.5}PW$, (b) $(NH_4)_1Cs_{1.5}H_{0.5}PW$, (c) $(NH_4)_{1.5}Cs_1H_{0.5}PW$ and (d) $(NH_4)_2Cs_{0.5}H_{0.5}PW$.

hydrogen bonding, forming adducts such as $Py–H^+\cdots Py$. This type of vibrational band was also observed in the FTIR spectrum of pyridine adsorbed on HZSM-5 [31] and on H_3PW [32]. In addition, the intensity of the bands related to Brønsted sites increase slightly as the amount of ammonium in the mixed salts increases. The presence of exclusively Brønsted sites in the mixed salts is in agreement with other studies that reported only this type of site for the pure salts of $(NH_4)_xH_{3-x}PW$ and $Cs_xH_{3-x}PW$ [28,29].

To quantify the amount and strength of the sites detected by FTIR, a pyridine desorption experiment was prepared and followed by TG/DTG analysis. The DTG curve (Fig. 6) shows three mass losses: (i) in the range of 25–120 °C (maximum peak ~60 °C) related to the release of water physically adsorbed on the mixed salts; (ii) in the range of 410–520 °C (maximum at ~485 °C), pyridine desorbed from the weakest Brønsted sites; and (iii) in the range of 520–600 °C (maximum around 549 °C), pyridine is desorbed from the strongest Brønsted sites. Because the latter two events simultaneously involve decomposition of ammonium ions and decomposition of the Keggin anion, respectively, the calculation of the total amount of pyridine desorption considered these effects. Actually, the number of moles of pyridine adsorbed on the catalyst (n_{py}) was calculated by the difference between the DTG

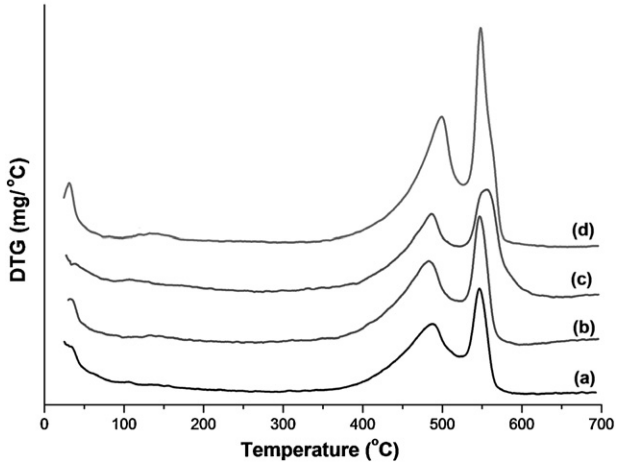

Fig. 6. DTG curves of the following mixed salts after pyridine adsorption treatment: (a) $(NH_4)_{0.5}Cs_2H_{0.5}PW$, (b) $(NH_4)_1Cs_{1.5}H_{0.5}PW$, (c) $(NH_4)_{1.5}Cs_1H_{0.5}PW$ and (d) $(NH_4)_2Cs_{0.5}H_{0.5}PW$.

curve of the mixed salts with and without pyridine for each mass loss, according to the method developed earlier [33] and explained by Eq. (5).

Preliminary FTIR results suggested that the total amount of Brønsted sites increased slightly with an increase in ammonium content. Considering that the mixed salts have about the same amount of protons (0.5 mol per mol of salt, within the experimental error), the total acidity as determined by TGA/DTA shows that not all protons have the same accessibility to pyridine molecules (Table 1). Actually, the number of sites probed by pyridine is about twice the number of protons obtained by the stoichiometric formula (average of 0.164 mmol g^{-1} of catalyst). This is consistent with the FTIR spectra of pyridine adducts with mixed salts, which showed the formation of hydrogen-bonded pyridine with a 2:1 ratio ($Py–H^+\cdots Py$) in the protonic site. The higher accessibility of pyridine to the protons of the salt $(NH_4)_2Cs_{0.5}H_{0.5}PW$ may be related to its higher specific surface area and average pore size. Pyridine is a small molecule that is able to reach all of the protons in the secondary structure of the mixed POMs. However, a larger and less basic molecule may have more restrictions to react with the active sites of these catalysts. Indeed, this was tested by an esterification reaction.

3.4. Catalytic esterification

Esterification reactions have low equilibrium constants and require the addition of an acid catalyst to reach high yields in a reasonable amount of time. Although esterification can be conducted using either Lewis or Brønsted acid, the later is more frequent [6,8]. Because oleic acid is one of the important components of many vegetable oils (e.g., 27 wt% in soybean oil), it was chosen as a model reagent to measure the activity of these mixed salts, with sights on further applications in soybean soapstock.

Esterification reactions are usually tested under a large excess of alcohol to achieve higher conversions. Based on other studies developed in our laboratory [6,8,20], the reaction was tested with three different ratios of oleic acid to ethanol: 1:30, 1:15 and 1:6. These studies were also followed at different reaction times at a fixed temperature (80 °C) and amount of catalyst (10 wt% related to limiting reactant, i.e., oleic acid). An increase in the conversion of oleic acid to ethyl oleate is observed at longer times, as is expected for an esterification reaction, and also with lower oleic acid to ethanol ratios (Fig. 7). Although it was expected that an increase in ethanol would produce more ester because of the Le Chatelier equilibrium effect, the best results with a 1:6 molar ratio can be explained based on the mechanism of the esterification reaction in the presence of a heterogeneous catalyst. The protonation of the acyl group that belongs to the carboxylic acid gives rise to the formation of a carbocation, which is attacked by the alcohol nucleophile. The intermediate with tetra-coordinated structure eliminates water to produce the ester (ethyl oleate) and to liberate the catalyst for another cycle. This reaction takes place on the catalyst surfaces. Both reactants could be adsorbed on the active sites of the catalyst to further react and desorb the products, or only the acid could be adsorbed, which leads the alcohol molecule to attack the carbocation from the solution. The amount of ethanol at higher molar ratios limits the interaction of the acid with the catalyst, saturating the surface active sites and leading to a limiting rate of the reaction kinetics. This effect has been observed by other researchers [34–36].

In addition, the conversion correlates reasonable well with acidic characterization results, i.e., the ratio of conversion increases monotonically as the amount and accessibility of the acid sites increases. Nonetheless, to compare the intrinsic catalytic activity of each material, the reaction kinetics should be measured at a low conversion range. The best method involved the curve fitting of the

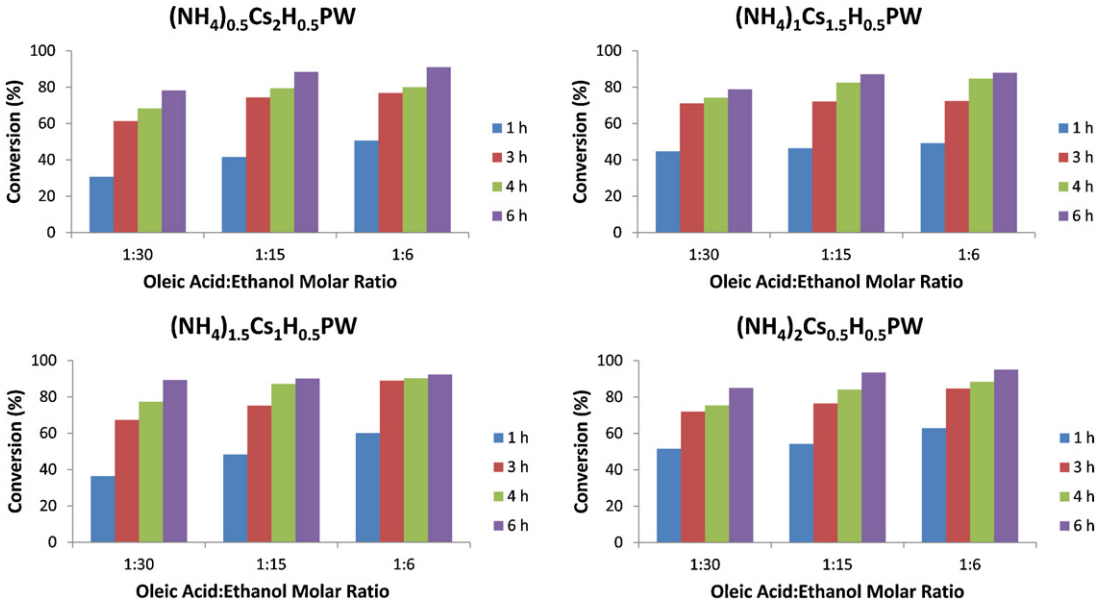

Fig. 7. Effects of the molar ratio of reactants in the conversion of oleic acid with ethanol. The conditions used included: 80 °C and 10 wt% catalyst in relation to the acid.

plot of ester produced (mmol) versus time (s) to a third-order polynomial function. This function was differentiated, evaluated at $t = 0$ and divided by the number of theoretical protons of each catalyst (Table 1). This calculation based on the amount of protons is probably the most reliable method because it considers the maximum amount of active sites per gram of catalyst. Besides, the larger size of oleic acid compared to pyridine implies that no more than one acid molecule is likely to interact with each proton. Thus, the highest activity of the mixed salts belongs to $(NH_4)_2Cs_{0.5}H_{0.5}PW$, which is in agreement with the previous evaluation using conversion values.

The slightly higher value of TOF for $(NH_4)_2Cs_{0.5}H_{0.5}PW$ indicates the high accessibility of the reactants to the secondary structure of this mixed salt. This is probably due to the highest surface area, pore size and pore volume of this mixed salt and mainly the amount of mesopores in the structure. According to Table 1, the $(NH_4)_2Cs_{0.5}H_{0.5}PW$ has the highest contribution of mesopores in the series, based on the difference between BET surface area and micropore area (52.9% for $(NH_4)_2Cs_{0.5}H_{0.5}PW$ versus 19.4% for $(NH_4)_{0.5}Cs_{1.5}H_{0.5}PW$), and has the highest average pore size (3.4 nm). Thus, these set of textural properties may explain the better accessibility of the protons in the secondary structure of this mixed salt for the attack of the carboxylic acid and, as a result, a higher activity.

The esterification reaction is a homogeneous process for pure H_3PW because it is very soluble in ethanol. The data included in Table 1 were obtained in a saturated solution of H_3PW in ethanol (about 1:1 mass ratio H_3PW:ethanol) and the same oleic acid:ethanol molar ratio (1:6) [8]. The TOF was recalculated according to the method explained in Section 2.5. The reaction was very fast in these conditions and was complete in less than 1 h. Even with less H_3PW (e.g., about 10 wt% in relation to oleic acid), a conversion of 99% was reached in 1 h. Thus, the best mixed salt, $(NH_4)_2Cs_{0.5}H_{0.5}PW$, is very efficient in a proton base quantity, i.e., it uses less hydrogen per mol, and has the advantages of a heterogeneous system.

In addition, a test in the solution [37] to make sure that only heterogeneous catalysis was involved was carried out (data not shown). For the mixture containing $(NH_4)_2Cs_{0.5}H_{0.5}PW$ catalyst, the reaction was left for 1 h (under the same experimental conditions described above). The catalyst was filtrated out and the solution was allowed to react up to 6 h. It was found that there was no change in the conversion (~63%) of oleic acid (i.e., the same conversion was obtained at 1 h and 6 h). Thus, no contribution of homogeneous catalysis was detectable.

3.5. Recycling and leaching tests of the catalysts

To evaluate the recycling potential of the prepared materials, the catalyst $(NH_4)_2Cs_{0.5}H_{0.5}PW$ was chosen because of the best activity in oleic-acid conversion. The catalyst was submitted to six reaction cycles. It was recovered by centrifugation (96–98%), washed with ethanol, dried in an oven at 150 °C, calcined at 300 °C for 4 h (right before the reaction), weighed and reinserted into the reaction system. The reaction conditions included: 1 h; 80 °C; molar ratio acid:ethanol = 1:6; 10 wt% catalyst. The results showed that the activity measured by the conversion of oleic acid was practically constant (average = 62.9 ± 1.2%) for these tests. The accuracy of these data was obtained by replenishing with fresh catalyst in each cycle, based on the mass recovered.

Another important issue related to POMs is solubility. The solubility was tested by a previously described procedure [8]; no solubility in oleic acid was detected by UV–vis method; the catalyst was suspended in ethanol, and the solution was sampled for analysis at regular intervals (10 min). The analysis, carried out by UV–vis spectrophotometry, used an analytical curve ($A = 4.2709 \times 10^4[H_3PW] + 0.2542$, $\lambda = 263$ nm, $R^2 = 0.9998$). No significant leaching (~1%) was detected for $(NH_4)_2Cs_{0.5}H_{0.5}PW$ up to 1 h. A longer measurement at 6 h did not show any increase in the concentration of the Keggin anion in ethanol (data not shown). This result is also compatible with that obtained for $Cs_xH_{3-x}PW$, which showed very low leaching [9] and confirms the insoluble nature of these salts. This certainly helps to explain the good reproducibility of the conversion results during reutilization of this catalyst.

4. Conclusions

This work described the preparation of a series of mixed salt derivatives of $H_3PW_{12}O_{40}$ (H_3PW) by the precipitation/ion exchange method (addition of $(NH_4)_2CO_3$ to H_3PW followed by Cs_2CO_3, leading to the salts $(NH_4)_xCs_{2.5-x}H_{0.5}PW$, $x = 0.5, 1, 1.5, 2$). The maintenance of the Keggin structure was confirmed by FTIR and FT-Raman. The thermal stability of these mixed salts must be

considered in relation to the entire composition and to the decomposition of the Keggin anion. Decomposition of ammonium is observed above 350 °C, whereas the Keggin anion began to degrade above 520 °C. These salts are much more stable than pure H_3PW, but calcination up to 300 °C is recommended to maintain their total integrity, i.e., including the ammonium composition and no loss of protons by association with structural lattice oxygen. In addition, the gaseous desorption of pyridine probed by TGA/DTG demonstrated the formation of Py–$H^+\cdots$Py adducts, which accounted for the double amount of protons expected in each salt. The nature of the acidic sites were probed by pyridine adsorption and detected by FTIR, which showed the presence of Brønsted sites only. The accessibility effect of the protons on those mixed salts was evaluated by the esterification reaction of oleic acid with ethanol. The best conditions were a 1:6 oleic acid:ethanol molar ratio and 10 wt% catalyst (in relation to the acid). The most efficient salt was $(NH_4)_2Cs_{0.5}H_{0.5}PW$ with TOF = 1.314 $mol_{EO}\ mol^{-1}\ proton\ s^{-1}$, which had the highest BET specific surface area (46.1 $m^2\ g^{-1}$), the highest average pore size (3.4 nm) and the highest distribution of mesopores (~53%) in the series. This catalyst was reutilized six times with average conversion of 62.9 ± 1.2% for an hour reaction.

Acknowledgments

We acknowledge CNPq for research, doctorate and undergraduate scholarships and the financial support provided by UnB/DPP/IQ, CAPES, FINATEC, FAPDF, MCT/CNPq, FINEP/CTPetro and FINEP/CTInfra.

Appendix A. Supplementary data

Supplementary data associated with this article can be found, in the online version, at http://dx.doi.org/10.1016/j.apcata.2012.07.013.

References

[1] D.L. Long, R. Tsunashima, L. Cronin, Angew. Chem. Int. Ed. 49 (2010) 1736–1758.
[2] M.M. Heravi, S. Sadjadi, J. Iran. Chem. Soc. 6 (2009) 1–54.
[3] M. Misono, Catal. Today 144 (2009) 285–291.
[4] R.S. Drago, J.A. Dias, T.O. Maier, J. Am. Chem. Soc. 119 (1997) 7702–7710.
[5] F. Ma, M.A. Hanna, Bioresour. Technol. 70 (1999) 1–15.
[6] G.F. Ghesti, J.L. Macedo, V.C.I. Parente, J.A. Dias, S.C.L. Dias, Appl. Catal. A 355 (2009) 139–147.
[7] J.R. Bartle, A. Abadi, Energy Fuels 24 (2010) 2–9.
[8] C.F. Oliveira, L.M. Dezaneti, F.A.C. Garcia, J.L. de Macedo, J.A. Dias, S.C.L. Dias, K.S.P. Alvim, Appl. Catal. A 372 (2010) 153–161.
[9] A. Alsalme, E.F. Kozhevnikova, I.V. Kozhevnikov, Appl. Catal. A 349 (2008) 170–176.
[10] B.Y. Giri, N. Rao, B.L.A.P. Devi, N. Linquiab, I. Suryanarayana, R.B.N. Prasad, Catal. Commun. 6 (2005) 788–792.
[11] M.G. Kulkarni, R. Gopinath, L.C. Meher, A.K. Dalai, Green Chem. 8 (2006) 1056–1062.
[12] P. Morin, B. Hamad, G. Sapaly, M.G.C. Rocha, P.G.P. de Oliveira, W.A. Gonzalez, E.A. Sales, N. Essayem, Appl. Catal. A 330 (2007) 69–76.
[13] K. Narasimharao, D.R. Brown, A.F. Lee, A.D. Newman, P.F. Siril, S.J. Tavener, K. Wilson, J. Catal. 248 (2007) 226–234.
[14] F. Chai, F. Cao, F. Zhai, Y. Chen, X. Wang, Z. Su, Adv. Synth. Catal. 349 (2007) 1057–1062.
[15] G. Sunita, B.M. Devassy, A. Vinu, D.P. Sawant, V.V. Balasubramanian, S.B. Halligudi, Catal. Commun. 9 (2008) 676–702.
[16] A.L. Cardoso, R. Augusti, M.J. Da Silva, J. Am. Oil Chem. Soc. 85 (2008) 555–560.
[17] C.S. Caetano, I.M. Fonseca, A.M. Ramos, J. Vital, J.E. Castanheiro, Catal. Commun. 9 (2008) 1996–1999.
[18] L. Xu, X. Yang, X. Yu, Y. Guo, Maynurkader, Catal. Commun. 9 (2008) 1607–1611.
[19] J.S. Santos, J.A. Dias, S.C.L. Dias, F.A.C. Garcia, J.L. Macedo, F.S.G. Sousa, L.S. Almeida, Appl. Catal. A 394 (2011) 138–148.
[20] G.F. Ghesti, J.L. Macedo, V.S. Braga, A.T.C.P. Souza, V.C.I. Parente, E.S. Figuerêdo, I.S. Resck, J.A. Dias, S.C.L. Dias, J. Am. Oil Chem. Soc. 83 (2006) 597–601.
[21] E. Caliman, J.A. Dias, S.C.L. Dias, F.A.C. Garcia, J.L. Macedo, L.S. Almeida, Micropor. Mesopor. Mater. 132 (2010) 103–111.
[22] C. Rocchiccioli-Deltcheff, M. Fournier, R. Franck, R. Thouvenot, Inorg. Chem. 22 (1983) 207–216.
[23] C. Rocchiccioli-Deltcheff, R. Thouvenot, R. Franck, Spectrochim. Acta A 32 (1976) 587–597.
[24] J.A. Dias, M.C. Rangel, S.C.L. Dias, E. Caliman, F.A.C. Garcia, Appl. Catal. A 328 (2007) 189–194.
[25] F. Lefebvre, F.X. Liu-Cai, A. Auroux, J. Mater. Chem. 4 (1994) 125–131.
[26] J.A. Dias, S.C.L. Dias, N.E. Kob, J. Chem. Soc., Dalton Trans. 3 (2001) 228–231.
[27] B.W.L. Southward, J.S. Vaughan, C.T. O'Connor, J. Catal. 153 (1995) 293–303.
[28] A. Corma, A. Martínez, C. Martínez, J. Catal. 164 (1996) 422–432.
[29] J.A. Dias, E. Caliman, S.C.L. Dias, Micropor. Mesopor. Mater. 76 (2004) 221–232.
[30] E.P. Parry, J. Catal. 2 (1963) 371–379.
[31] R. Buzzoni, S. Bordiga, G. Ricchiardi, C. Lamberti, A. Zecchina, Langmuir 12 (1996) 930–940.
[32] A. Vimont, A. Travert, C. Binet, C. Pichon, P. Mialane, F. Sécheresse, J.-C. Lavalley, J. Catal. 241 (2006) 221–224.
[33] F.A.C. Garcia, V.S. Braga, J.C.M. Silva, J.A. Dias, S.C.L. Dias, J.L.B. Davo, Catal. Lett. 119 (2007) 101–107.
[34] S. Malik, S.S. Dash, K.M. Parida, B.K. Mohapatra, J. Colloid Interface Sci. 300 (2006) 237–243.
[35] S.R. Kirumakki, N. Nagaraju, S. Narayanan, Appl. Catal. A 273 (2004) 1–9.
[36] B.R. Jermy, A. Pandurangan, J. Mol. Catal. A: Chem. 237 (2005) 146–154.
[37] V. Brahmkhatri, A. Patel, Appl. Catal. A: Gen. 403 (2011) 161–172.